Available online at www.sciencedirect.com

SciVerse ScienceDirect

Ceramics International 39 (2013) 4489–4497

CERAMICS INTERNATIONAL

www.elsevier.com/locate/ceramint

Theoretical and experimental investigations on the mechanism of carbothermal reduction of zirconia

A. Sondhi, C. Morandi[1], R.F. Reidy*, T.W. Scharf

Department of Materials Science & Engineering and Institute for Science and Engineering Simulation (ISES), University of North Texas, Denton, TX 76207, USA

Received 7 September 2012; received in revised form 31 October 2012; accepted 16 November 2012
Available online 10 December 2012

Abstract

Zirconium carbide (ZrC) is an important ultra-high temperature ceramic due to its refractory properties. It is commonly synthesized via carbothermal reduction of zirconia above 1657 °C according to the reaction ZrO_2 (s)+3C (s)→ZrC (s)+2CO (g). Contrary to this reaction, prior research indicates that carbon monoxide (CO) is the responsible species for carburizing ZrO_2 to form ZrC. To explore this reaction pathway, investigations were performed by making two mixed phase pellets with 3 mol% yttria-stabilized zirconia (YSZ) and graphite. Both had an upper half made of YSZ. The lower half of one sample consisted of finely mixed YSZ and graphite powder whereas the other was pure graphite. Similar experiments were conducted with sintered YSZ pellets on top. After heat treatment at 1800 °C, X-ray diffraction analysis revealed higher ZrC conversion for the YSZ pellet face in direct contact with pure graphite. This contradicts the previous work as one would assume higher ZrC yield for YSZ pellet in direct contact with YSZ/graphite mix as they produce more CO upon reaction. Lastly, diffusional experiments showed conversion to be highly localized to a depth of ~25 μm. This is in close agreement with calculations for carbon diffusion in YSZ based on a diffusion coefficient (D)=3×10^{-14} m^2/s, which confirms solid–solid reaction rather than solid–gas reaction.

Keywords: Carbothermal reduction; Carbon diffusion; Ultra-high temperature ceramic; Zirconium carbide

1. Introduction

Zirconium carbide is known for its high melting temperature, 3400–3540 °C, high hardness, 2100 Knoop, and high modulus of elasticity, 380×10^9 Pa [1]. These properties enable it to be used in cutting tools, as a refractory material and in composites to impart high strength. It has also found applications in electronic devices [2] and as a low neutron absorbing material in the nuclear industry [3].

Carbothermal reduction is a common chemical process practiced commercially for the synthesis of many non-oxide ceramic powders. Zirconium carbide powders have long been produced by using carbothermal reduction under various conditions and surroundings [4,5]. The mechanism and species involved leading to carbide conversion has been studied since the early 1980s when Vodopyanov et. al. [6,7] reported that at high temperatures zirconia (ZrO_2) reacts with carbon monoxide (CO) to form carbides on the surface of oxides under non-vacuum conditions. In experiments conducted in inert atmospheres [8], ZrO_2 reacts with CO to form an oxycarbide phase, $ZrC_{0.9-x}O_x$ (x=0.04−0.08) that subsequently forms ZrC [9]. Absent from these studies is the dependence of CO partial pressure on this reaction. CO occurs as a reaction product during carbothermal reduction of zirconia at temperatures 1657 °C and above [10] according to

$$ZrO_2\ (s)+3C\ (s)\rightarrow ZrC\ (s)+2CO\ (g) \quad (1)$$

This reaction shows that the CO available for reaction with zirconia is dependent on the prior carbothermal reduction of ZrO_2. Moreover, CO is a larger species than C which precludes its diffusion in zirconia.

*Correspondence to: North Texas Discovery Park, Room No. E108, 3940 North Elm St., Denton, TX 76207, USA. Tel.: +1 940 369 7115.
E-mail address: reidy@unt.edu (R.F. Reidy).
[1]Current address: The Department of Materials Science and Engineering, The Pennsylvania State University.

0272-8842/$ - see front matter © 2012 Elsevier Ltd and Techna Group S.r.l. All rights reserved.
http://dx.doi.org/10.1016/j.ceramint.2012.11.043

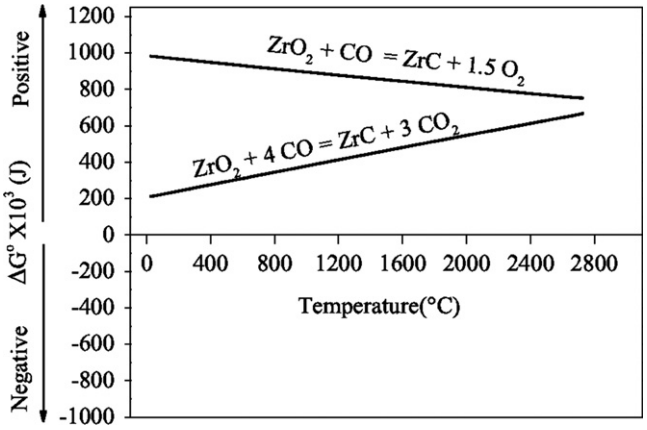

Fig. 1. Graph showing variation of change in standard Gibbs free energy (ΔG°) as a function of temperature for reactions (2) and (3).

Thermodynamic reactions involving CO and ZrO_2 indicate that ZrC is unlikely to form from these reactants. Fig. 1 shows change in Gibbs free energy (ΔG) plots for two different reactions (Eqs. (2) and (3)) between ZrO_2 and CO:

$$ZrO_2\ (s)+4CO\ (g)\rightarrow ZrC\ (s)+3CO_2\ (g) \quad (2)$$

$$ZrO_2\ (s)+CO\ (g)\rightarrow ZrC\ (s)+1.5O_2\ (g) \quad (3)$$

The ΔG values are highly positive for a large temperature range confirming that under atmospheric pressure CO is unlikely to react with ZrO_2 to form ZrC [11,12]. Reactions (2) and (3) can go in the forward direction only (i.e., have negative ΔG values) under non-equilibrium conditions. These values are governed by the following equation:

$$\Delta G=\Delta G^{\circ}+RT\ln Q \quad (4)$$

where ΔG° is change in Gibbs free energy at standard state, R is the gas constant, T is the absolute temperature, and Q is the reaction rate constant. Fig. 1 shows ΔG° is always positive for both reactions. Thus for ΔG to be negative, $\Delta G^{\circ} < -RT\ln Q$. Therefore, unless the partial pressures of CO are very high (1.9×10^{14} Pa at 25 °C for reaction (2)), CO will not convert ZrO_2 to ZrC. Moreover, under equilibrium conditions and unit activity of solids in reaction (1), partial pressure of CO is calculated to be 4×10^{5} Pa at 1800 °C. This makes it extremely difficult for CO to initiate any ZrO_2 to ZrC transformation.

In many reactions such as

$$2C\ (s)+O_2\ (g)\rightarrow 2CO\ (g) \quad (5)$$

Varied ratios of CO, CO_2 and O_2 can result in activity of carbon greater than one. Consequently, carbon would start depositing from atmosphere. Our system, graphite furnace, had a partial pressure of O_2 at ~0.09 Pa. A quick analysis would reveal that unless the partial pressure of O_2 is not less than $\sim3.13\times10^{-9}$ Pa, the activity of graphite would not exceed a value of one according to reaction (5) [11,12]. Therefore, the main motivation of this study is to examine the extent of reaction and potential mechanisms of zirconia carbothermal reduction under differing exposures to carbonaceous species—namely CO and C.

2. Experimental procedure

2.1. Sample preparation

A composite pellet system was designed that consisted of two parts: upper and lower halves which were made separately by die pressing powders to form pellets. The YSZ powder was manufactured by Tosoh Corporation under product name TZ-3Y-E. The 3 mol% YSZ exhibited specific area of 15,200 m^2/kg and crystallite size of ~26 nm. The graphite powder (300 mesh size) was produced by Alfa Aesar. The motivation behind constructing a composite system was to use the bottom half of the pellet as a source of CO and/or C for reactions to occur into and within the top half. Fig. 2 shows the two composite systems, MP and GP, and their sintered counterparts, MPs and GPs. The naming convention is based upon the nature of bottom half of the pellet systems. MP and MPs have a mixed bottom pellet made from YSZ and graphite. Thus a designation "MP" is used to abbreviate "mixed pellet". Similarly GP and GPs pellet systems have their bottom half made up of graphite only, and thus follow the abbreviation "GP" which stands for "graphite pellet". MPs and GPs have an added suffix "s" since their top half, YSZ, was sintered before being put on its bottom half. Four pellet systems, with multiple repetitions have been tested which yielded reproducible results.

MP consisted of a bottom half made up of YSZ and graphite mixed using a mortar and pestle in a molar ratio of 1:3.3. This powder blend was then die pressed at uniaxial pressure of 34.4×10^{6} Pa to form a cylindrical shaped pellet. The GP pellet consisted of a bottom half made only from 0.25 g graphite powder. Both top halves for MP and GP were made up of 1 g of YSZ powder again die pressed to cylindrical pellet of density ~2940 kg/m^3. In MPs and GPs samples, the YSZ top half was sintered after die pressing to a density of 5800 kg/m^3 (~96.7% dense) prior to putting in for reaction heat treatment. The sintering temperature–time profile is shown in Fig. 3. In none of the samples discussed above were the top half and bottom half die pressed together. Top half of any pellet system was simply placed on top of its respective bottom half by means of a tweezer.

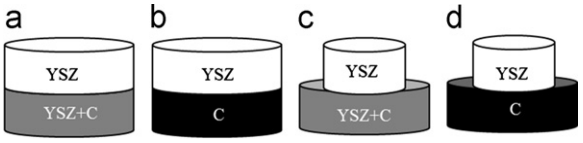

Fig. 2. Schematics of pellets: (a) MP, (b) GP, (c) MPs, and (d) GPs. Shrinkage seen in top half of MPs and GPs is due to prior sintering of the YSZ pellet.

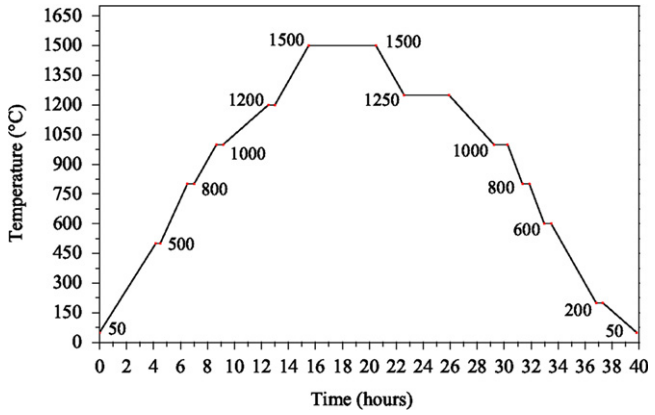

Fig. 3. Heat treatment procedure for sintering top halves of GPs and MPs. Each labeled data point shows corresponding temperature at various hold stages.

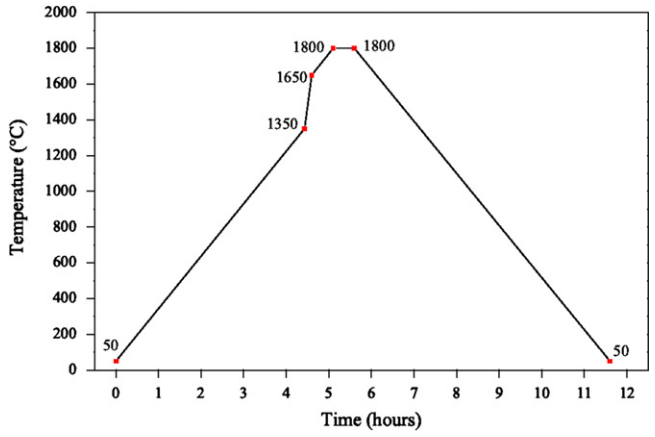

Fig. 4. Carbothermal reduction heat treatment procedure for MP, GP, MPs and GPs. Numbers next to data points indicate corresponding temperature.

2.2. Carbothermal reduction heat treatments

Heat treatments were done under flowing helium in a Thermal Technology graphite furnace (Model 1000-2560-FP20). Prior to heat treatments, the chamber was pumped down to $\sim 1.3 \times 10^{-4}$ Pa base pressure and then flushed with research grade He. Samples were heated to a temperature of 1800 °C under flowing He by using the procedure shown in Fig. 4. This involved a ramp up from room temperature to 1350 °C at a rate of 300 °C/h, from 1350 °C to 1650 °C at a rate of 1800 °C/h, from 1650 °C to 1800 °C at a rate of 300 °C/h, followed by a dwell of 1800 s and cooling down to 20 °C at a rate of 300 °C/h.

2.3. Characterization

Cu-Kα X-ray diffraction (XRD) was done using a Rigaku Ultima III diffractometer. Scans were acquired from top and bottom halves of all the pellets before and after heat treatments. These were then analyzed for the phases present and their respective mole fractions. Peak identification corresponding to YSZ, graphite and zirconium carbide were done using JCPDS files nos. 01-070-4426, 01-071-4630 and 01-073-0477, respectively. MDI Jade software was used for peak identification and Reitveld refinement on all XRD scans to obtain molar percentages of various phases.

3. Results and discussion

3.1. Characterization of pellets before and after carbothermal reduction heat treatment

XRD determined that the 3 mol% YSZ raw powder consisted of tetragonal and monoclinic zirconia phases as shown in Fig. 5. The basic aim behind designing the four composite pellet systems was to diffuse relative amounts of CO and C as minor and major species into their respective YSZ top halves. Based on reaction (1), the MP bottom half pellet would form ZrC and liberate CO at $T > 1657$ °C. This CO along with some C is then available to react with the top half of the pellet. Due to a mixed bottom half in MP, CO, in principle, is the primary diffusional species. GP has a bottom half composed only of graphite. Thus, C, in principle, would be the primary species diffusing into its top half. Therefore, CO generation due to the YSZ and graphite reaction at interface on top and bottom half would be considerably less in GP as compared to the MP pellet. As a result, C would be a more abundant diffusional species in GP than CO. Moreover, during heat treatment the top halves would undergo phase transformation, to ZrC, and sintering, to 80% density of zirconia, at the same time. This would concurrently reduce porosity and retard any CO diffusion owing to its bigger size.

MPs and GPs, have the same bottom halves as MP and GP, respectively, but the YSZ top halves are sintered to 98% of the theoretical density of zirconia before reaction heat treatment. CO gas diffusion would thus be limited in

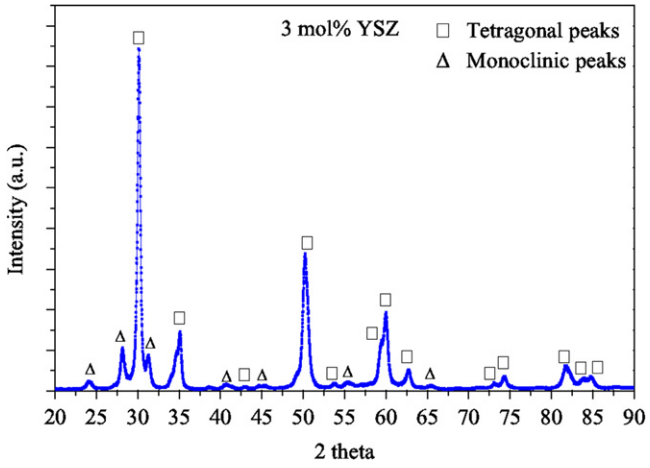

Fig. 5. XRD scan of starting YSZ powder showing primarily tetragonal zirconia with some monoclinic zirconia.

sintered YSZ since there is negligible porosity limiting diffusion of the larger CO molecule. Like in MP, the primary species available for reaction with ZrO_2 in MPs is CO while C is much less abundant. In GPs the primary abundant species for diffusion is C whereas CO would be the minor species.

At the carbothermal reduction heat treatment temperature of 1800 °C, C and CO can diffuse from the bottom half of a pellet (source) into its respective top half (sink). Even with increased mobility of these species, carbothermal reduction will occur only at temperatures where reaction (1) has negative values of the Gibbs free energy. The bottom half of each pellet serves as a carbon source, in minor and major amounts depending on the pellet system, for its respective YSZ top half. As previously mentioned, MP and GP have different dominant carbon species available to react with the top halves. MP has gaseous CO in abundance while GP provides only C as a reactant, at least initially. As the gaseous species becomes available, it can react with both faces and sides of the YSZ top half. However, in the GP pellet, solid carbon is in contact with YSZ and should result in a more solid diffusion based reaction.

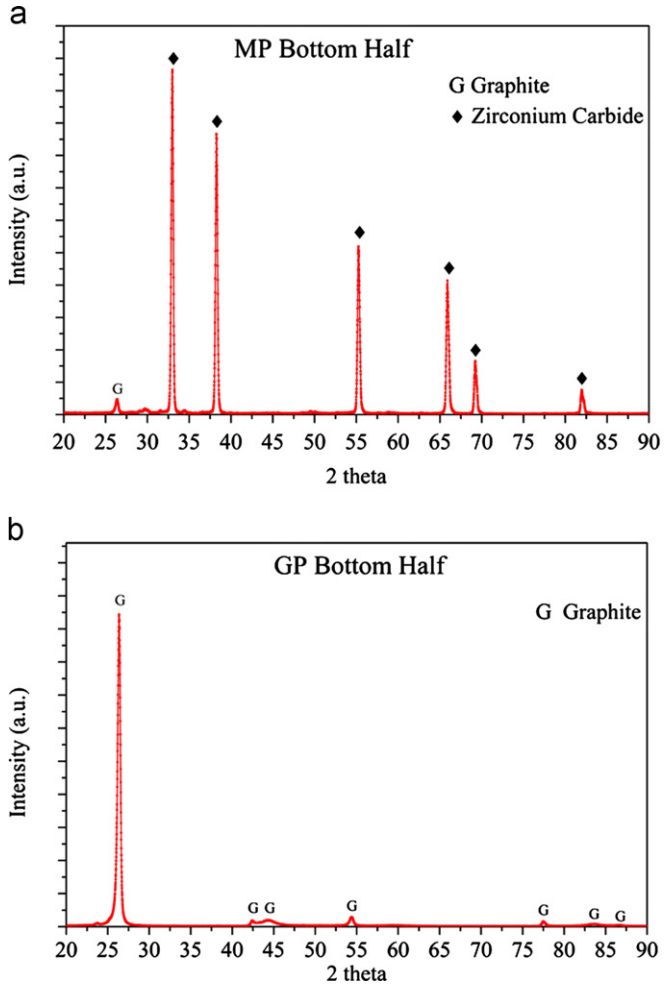

Fig. 6. XRD scans acquired from the bottom halves of (a) MP and (b) GP after carbothermal reduction heat treatment.

To differentiate amongst these possible reactions, separate XRD scans were acquired from the bottom and top halves. Fig. 6(a) shows XRD results acquired from the bottom half of MP. There are no peaks corresponding to YSZ confirming full conversion to ZrC. Although not shown, MPs exhibited the same XRD peaks. Conversely, the XRD results on GP, shown in Fig. 6(b), and GPs (not shown) exhibited only graphite peaks with no peaks corresponding to YSZ or ZrC. To characterize the top halves of the MP, GP, MPs, and GPs pellets, both its top and bottom faces were analyzed according to the procedure shown in Fig. 7. The corresponding XRD scans in Fig. 8 all show the presence of tetragonal ZrO_2 and ZrC in varying percentages, but with no presence of monoclinic ZrO_2. In Table 1, quantitative Reitveld refinement analyses show maximum ZrC conversion occurred for the bottom face of GP pellet followed by the GPs, MP and MPs pellets. The reason for this trend is because the GP pellets are a greater source of C, and, thus show a larger amount of ZrC formation. Meanwhile, the sintered samples show less ZrC formation than their un-sintered counterparts because sintering severely limits exposed interior surfaces as potential reaction sites. In addition, the lattice parameter for ZrC formed on various faces of the pellets is relatively constant, listed in Table 2, with an average around 4.673 Å and a standard deviation of 0.002 Å.

3.2. Bulk diffusion of C in YSZ pellets

The carbon diffusion coefficient in zirconia has been reported to be six orders of magnitude smaller than oxygen self-diffusion [13]. This would indicate several orders of magnitude difference in diffusivity between C and CO through YSZ due to the gaseous nature of CO. Based on the recent work of Vykhodets et al. [13] and utilizing their data, the diffusion coefficient of C in YSZ at 1800 °C is calculated to be 3×10^{-14} m^2/s [13]. Using Fick's second law and this diffusion coefficient, the effective diffusion length of C in YSZ can be approximated to 25 μm for 1800 s at 1800 °C (calculated plots shown in Fig. 9). According to these results at distances greater than 25 μm there should not be any ZrC formation due to lack of diffusing carbon. To confirm this experimentally, the top halves of MP, GP, MPs, and GPs were sliced radially to half their heights (~1.5 mm), shown in Fig. 10. After slicing, the XRD scans were acquired from the exposed faces, namely Faces A and B while keeping the X-ray beam close to the geometric center. Fig. 11 shows the XRD scans obtained from Faces A and B for all the pellets. None of the scans show the dominant ZrC (111) peak at $2\theta = 33.2°$. On the contrary, all the peaks correspond to YSZ (monoclinic and tetragonal phases) confirming that no ZrC formed in the center, at least to these 1.5–2 mm depths. Fig. 9 theoretically shows for longer diffusion times of 3600 s (circles)

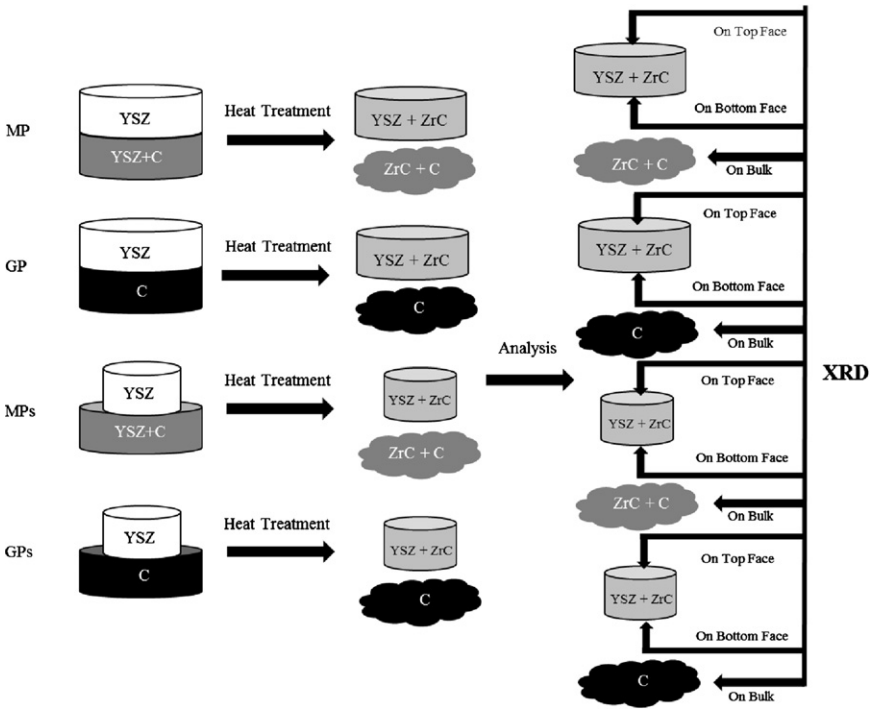

Fig. 7. Flowchart showing the methodology in XRD analysis of pellets before and after carbothermal reduction heat treatment. The cloud shape represents powder formed from bottom halves as they decompose after heat treatment.

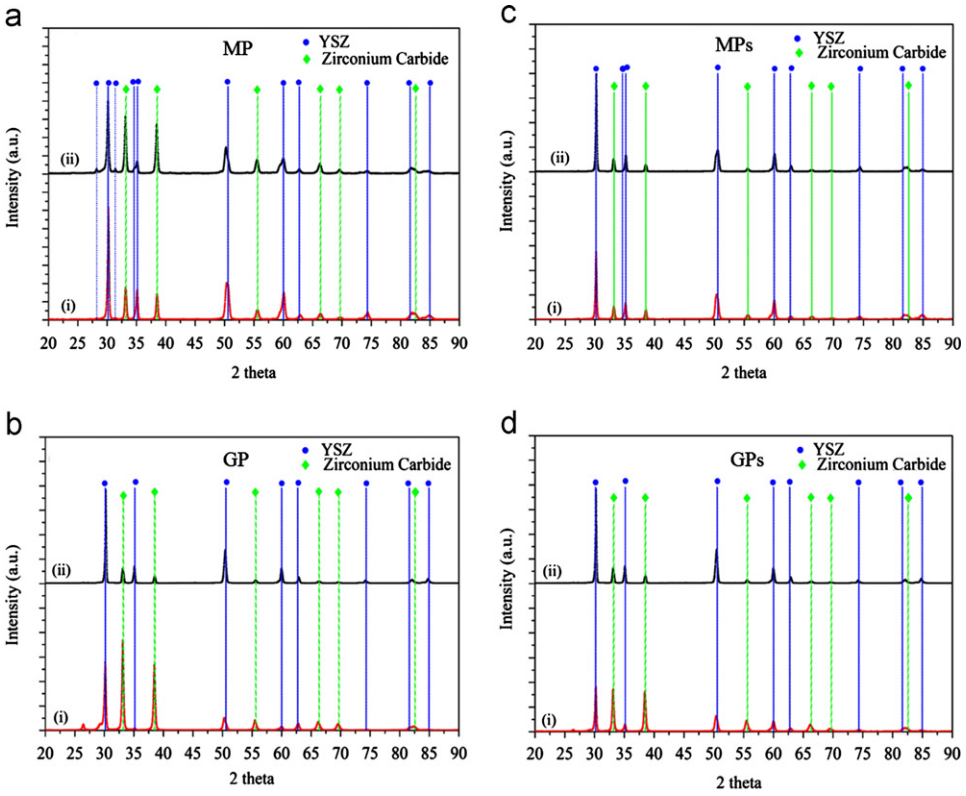

Fig. 8. XRD data acquired from (i) bottom face and (ii) top face of (a) MP, (b) GP, (c) MPs, and (d) GPs top half pellets. Table 1 lists the various amounts of ZrC formed on respective faces.

to 5400 s (triangles), C cannot diffuse past 50 μm distance. These results further confirm that carbothermal reduction is more C driven than CO driven due to its slow diffusional nature. X-ray penetration depth calculations indicate that the diffraction analysis only examines approximately the first 16–20 μm of ZrO_2/ZrC.

Table 1
Mole percentages of zirconium carbide formed on the top and bottom faces of respective top halves of MP, GP, MPs and GPs. These mole percentages were calculated by doing Rietveld analysis on the XRD data in Fig. 8.

Sample name	Mole percentages
MP	Top face—42% ZrC
	Bottom face—23% ZrC
GP	Top face—45% ZrC
	Bottom face—74% ZrC
MPs	Top face—15% ZrC
	Bottom face—18% ZrC
GPs	Top face—18% ZrC
	Bottom face—57% ZrC

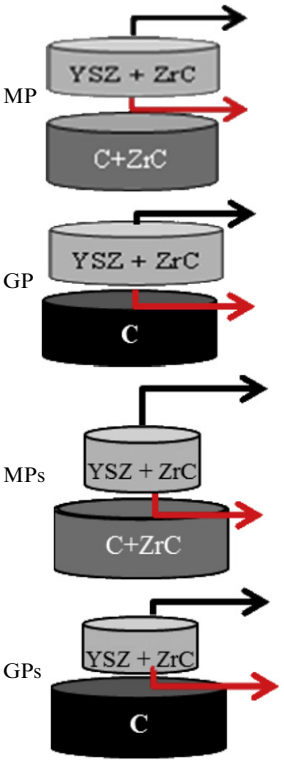

Table 2
Lattice parameters of zirconium carbide formed at various faces of top halves of MP, GP, MPs and GPs calculated from the XRD data in Fig. 8.

Top half	*a* (Å)	
	Bottom face	Top face
MP	4.669	4.675
GP	4.676	4.672
MPs	4.669	4.672
GPs	4.676	4.675

3.3. Surface diffusion of C on YSZ pellets

As mentioned earlier, the bottom half of MP acts as a strong source of CO and a weak source of C for diffusion into the top half. In contrast, GP acts as a strong C source and a weak CO source for its top half. In principle, during the course of the carbothermal reduction reaction, it is feasible that CO as a reaction product can be liberated from the sample and potentially form a sheath around the top YSZ pellet leading to radially inward diffusion. Similarly, C due to being a small and relatively mobile species can also diffuse to the top from surface sites on the pellet edges. These pathways can possibly cause a gradient in the amount of YSZ converted to ZrC along the sides of

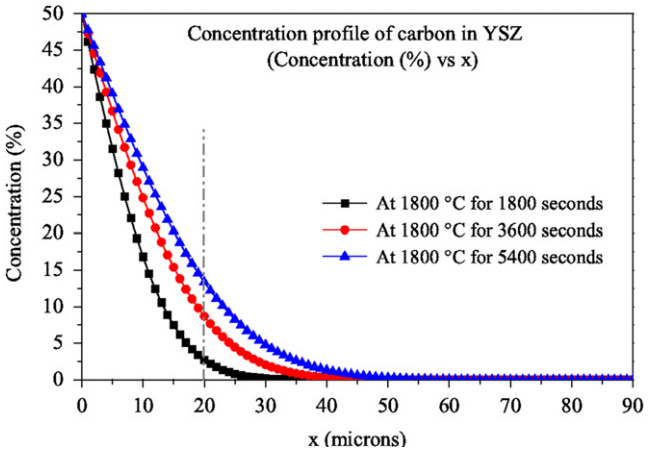

Fig. 9. Variation of carbon concentration as a function of diffusion distance (x) in YSZ at 1800 °C. Curves are plotted for various diffusion times of 1800, 3600 and 5400 s. Vertical dotted line shows maximum distance to which X-rays penetrated based on diffraction data acquired from bottom and top faces of MP, GP, MPs and GPs top halves.

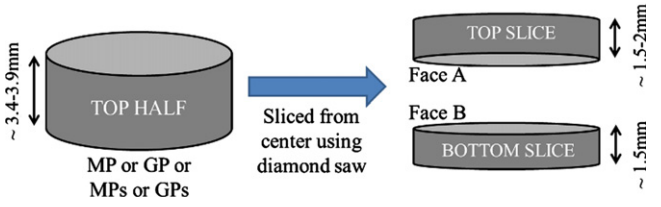

Fig. 10. Schematics of the methodology of slicing top halves of MP, GP, MPs and GPs along with approximate dimensions of original and sliced pellets. Faces A and B are labeled according to their geometric locations on sliced halves.

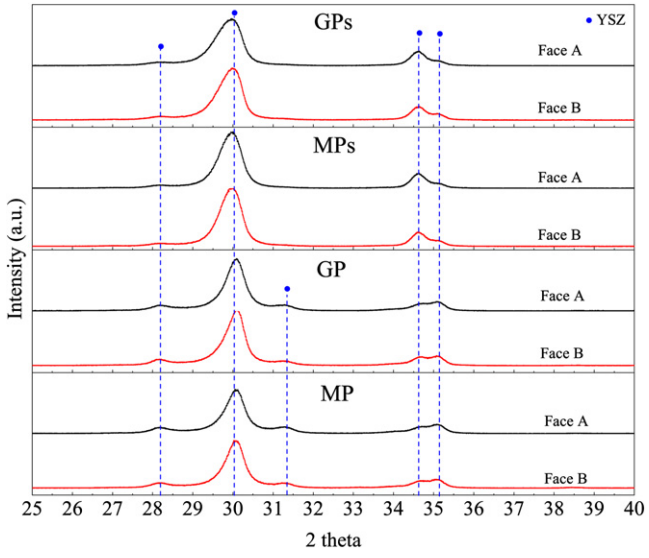

Fig. 11. XRD scans from Faces A and B (Fig. 10) of sliced MP, GP, MPs, and GPs top halves. No ZrC peak could be seen in any of the eight acquisitions.

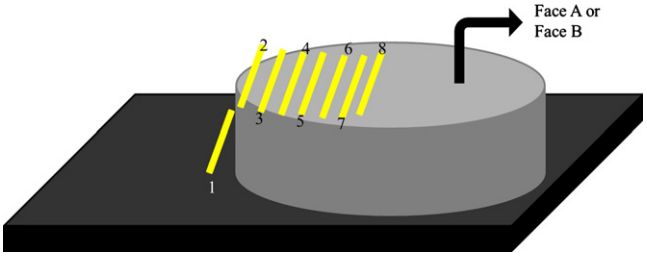

Fig. 12. Schematic of the various points for XRD measurements along the sliced face (A or B) of a top half pellet. Dark rectangular slab represents the XRD stage on which the pellet rests during acquisitions. The rectangular regions, designated by numbers 1–8, represent areas from where the XRD scans were obtained: point 1 is on the XRD stage which provides no diffraction, and points 2–8 span from the very edge of the pellet to near the pellet center.

the pellet in addition to the aforementioned bulk transformations occurring at respective bottom and top faces. Given the differences between gaseous and surface diffusion rates, one would expect that surface diffusion would have more observable time dependence. The physical inspection of the top halves after heat treatment showed color changes from bright white to gray to black indicating reactions occurred at the pellets' periphery.

Examination of these surface effects is important to understand details of the diffusion mechanism(s). To this end, a series of XRD spot scans were performed on one of the sliced faces (Face A or B) of the MPs and GPs pellets. These spot scans, when stitched together, form a line that connects the pellet edge to its center as shown in Fig. 12. Such a line scan can reveal a possible transition from ZrC to YSZ along the radial direction of the pellet. These XRD acquisitions, done using rectangular X-ray beam cross-sections, were made spatially large enough to cover considerable areas near the edge and center of the pellets' face.

XRD line scan results obtained from this procedure are shown in Fig. 13(a) for MPs and Fig. 13(b) for GPs. For both pellets, only YSZ peaks were detected with no evidence of ZrC reflections on all the XRD scans obtained from points 1–8. Since XRD has spatial limitations to detect small phase regions, XPS was employed to help determine the composition of the periphery of the pellet. These XPS results confirmed the presence of ZrC and a small concentration of yttrium within the ZrC layer.

Thus any surface diffusion occurring is significantly less than the previously observed bulk diffusion in the top and bottom faces of the MP, GP, MPs, and GPs top halves. Corresponding optical images of the X-ray spot streaks superimposed on actual samples are shown for MPs (Fig. 13(c)) and GPs (Fig. 13(d)).

3.4. Discussion on mechanism of carbothermal reduction of zirconia

During the carbothermal reduction heat treatment, the bottom face of the MP top half (YSZ) is exposed to more CO than GP because of its mixed ZrO_2 and C bottom half. Based on the previous research [6–9,14] where CO is thought to be the reaction driver for ZrC conversion, the bottom face of the MP top half should produce more ZrC formation than GP. However, it was determined that GP bottom face exhibits significantly more ZrC conversion (70%) than MP (23%). The pellet systems studied have CO and C as the only likely species capable of carburizing YSZ to ZrC. The top halves of MP and GP densify to 80% (4.8 g/cm^3). During this treatment, enough porosity exists that both species can diffuse; therefore, it is difficult to discern the dominating species driving carbide formation. To study this effect, sintered versions of these samples, GPs and MPs, were exposed to the same heat treatments and carbonaceous exposures as their porous counterparts. In both sintered samples, the top and bottom faces still show ZrO_2 to ZrC conversion, albeit less mole percent than the corresponding non-sintered pellets. These sintered YSZ top halves should, in principle, restrict or minimize any gaseous CO diffusion through them and only react through direct contact or gaseous species emanating from the lower halves. However, carbon because of its very small size can diffuse via grain boundaries, interstitial sites and lattice defect sites. Thus, reduction of YSZ to ZrC is still observed in the sintered GPs and MPs pellets.

Moreover, diffusion measurements [13] show that kinetics of carbon diffusion in zirconia is rather slow. Thus, any YSZ to ZrC conversion occurring because of carbon will be highly localized. Experimental XRD results on Faces A and B of the top halves confirms this since no ZrC was detected. In support of this, calculated X-ray depth penetration using procedure in Ref. [15] is less than 20 μm on bottom faces of all the pellets. This is in agreement with results and analysis from Vykhodets et al. [13] where carbon can diffuse only to depths of ~25 μm at 1800 °C, shown in Fig. 9. This effectively means that carbon diffusion in YSZ is so slow that it causes the diffusion front to extend to similar depths as that of the conversion front of ZrO_2 to ZrC transformation.

4. Summary and conclusions

Experiments and calculations were performed to determine carbothermal reduction mechanisms and whether CO is the dominant species driving the ZrO_2 to ZrC conversion. A series of experiments using pellet systems were conducted in which major and minor amounts of CO and C were exposed to YSZ, and the reaction products were analyzed to confirm the reaction driver. If CO is the source of C for ZrC formation then the sample with the most available CO, MP, would exhibit the highest conversion; however, this was not observed. Instead, GP, which has a bottom half of graphite acts as a weak source of CO, shows maximum ZrC formation at the interface between the top and bottom half due to solid–solid reaction of zirconia and graphite. In addition, the top halves of MP

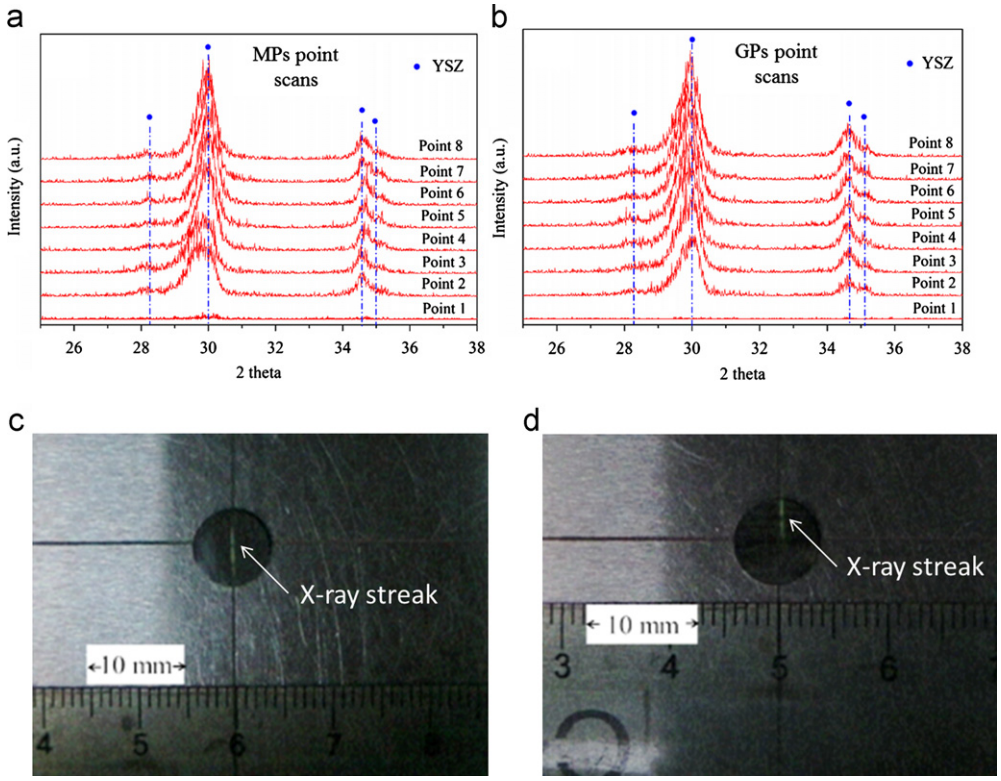

Fig. 13. Stacked XRD scans acquired from radially distributed points on Face A (or Face B) of sliced top halves of (a) MPs and (b) GPs pellets. No ZrC formation was detected along points 1–8. Point 1 corresponds to region near sample stage and point 8 corresponds to region near center of the sliced pellet. Optical images showing superimposed images of sliced (c) MPs and (d) GPs top halves with fluorescent streaks (denoted by arrows). Fluorescent streaks represent area where X-rays were falling on the sample during one of the acquisitions of points 1–8 on Face A or B. These were captured separately using same scale as that for sliced sample images and then superimposed on them.

and GP undergo sintering and reaction at the same time. This restricts CO diffusion through the bulk as the top pellets are sintered to 80% of theoretical density of zirconia during heat treatment. To form ZrC, a carbonaceous species must transport into ZrO_2, thus, C is a much more likely species to diffuse through a sintered sample than CO. In support of this mechanism, theoretical calculations indicate partial pressures of CO needed to drive zirconium carbide formation from zirconia are far beyond the environment in the reaction furnace. Since most of the processing is done under normal atmospheric pressure, so as to avoid capital investments and safety issues, formation of ZrC by reaction between ZrO_2 and CO appears less likely than carbon diffusion.

In addition, carbon diffusion in zirconia is slow even at elevated temperatures. Thus any ZrC formation is highly localized as seen experimentally in all the top halves as well as theoretically based on diffusion depth calculations. These results indicate carbothermal reduction to be C driven as CO would be expected to be orders of magnitude faster than C and cause unlocalized diffusion (within the sample pores). Based on the above, carbothermal reduction of zirconia is more dependent on solid–solid reaction than gas–solid reaction, which is in disagreement with previous research findings that suggest carbothermal reduction of zirconia to be only a CO driven reaction mechanism.

Acknowledgments

The authors would like to acknowledge the financial support from the US Air Force Research Laboratory (AFRL, ISES Contract no. FA8650-08-C-5226). We also acknowledge the use of the XRD facilities at the UNT Center for Advance Research and Technology (CART). In addition to this, we are very grateful to Dr. Srinivasan G. Srivilliputhur for helping edit this manuscript.

References

[1] C.A. Daniels, Data Section, in Ceramics: Structure and Properties, Abyss Books, Washington, DC, 2002, pp. 210–211.
[2] G. Montel, A. Lebugle, H. Pastor, Manufacture of Materials Containing Refractory Borides, Carbides, and Nitrides, and Their Application in Electronics and Electrical Engineering, Revue internationale des hautes temperatures et des refractaires 16 (1979) 95–124.
[3] G.V. Samsonov, Properties index, in: Handbook of High Temperature Materials, vol. 2, Plenum Press, New York, 1964, pp. 336–337.
[4] J.I. Kroschwitz, A. Seidel, Ceramics, industrial hard, in: J.I. Kroschwitz, A. Seidel (Eds.), Kirk-Othmer Encyclopedia of Chemical Technology, 5th ed., vol. 4, Wiley-Interscience, Hoboken, NJ, 2004, 694 pp.
[5] J.I. Kroschwitz, A. Seidel, Zirconium and zirconium compounds, in: A. Seidel (Ed.), Kirk-Othmer Encyclopedia of Chemical Technology, 5th ed., vol. 26, Wiley-Interscience, Hoboken, NJ, 2004, 640 pp.

[6] A.G. Vodopyanov, Role of thermodynamics in the process of reduction of metal oxides using carbon, Izvestiia Akademii nauk SSSR. Metally 5 (1981) 37–41.
[7] A.G. Vodopyanov, G.N. Kozhevnikov, S.V. Baranov, S.V. Zhidovinova, Mechanism of the carbothermic reduction of metals from heat-resistant oxides, Russian metallurgy. Metally 3 (1986) 1–10.
[8] A. Maitre, P. Lefort, Solid state reaction of zirconia with carbon, Solid State Ionics 104 (1997) 109–122.
[9] L.-M. Berger, W. Gruner, E. Langholf, S. Stolle, On the mechanism of carbothermal reduction processes of TiO_2 and ZrO_2, International Journal of Refractory Metals and Hard Materials 17 (1999) 235–243.
[10] A.W. Weimer, Carbide, Nitride and Boride Materials Synthesis and Processing, Chapman & Hall, London. New York, 1997.
[11] C.W. Bale, E. Bélisle, P. Chartrand, et al., FactSage thermochemical software and databases—recent developments, Calphad: Computer Coupling of Phase Diagrams and Thermochemistry 33 (2009) 295–311 〈http://www.sgte.org/reacweb.htm〉.
[12] M.W. Chase, United States. National Bureau of Standards, JANAF Thermochemical Tables, American Chemical Society, American Institute of Physics for the National Bureau of Standards, Washington, DC, New York, 1986.
[13] V. Vykhodets, T. Kurennykh, A. Kesarev, M. Kuznetsov, V. Kondrat'ev, C. Hülsen, U. Koester, Diffusion of insoluble carbon in zirconium oxides, JETP Letters 93 (2011) 5–9.
[14] W. Gruner, S. Stolle, L.-M. Berger, K. Wetzig, A new experimental approach for accelerated investigations of carbothermal reactions, International Journal of Refractory Metals and Hard Materials 17 (1999) 227–234.
[15] B.D. Cullity and S.R. Stock, Diffraction II: intensities of diffracted beams, in: Elements of X-ray Diffraction, Prentice-Hall, Upper Saddle River, NJ, 2001, pp. 152–154.